Close Proximity of Myosin Loop 3 to Troponin Determined by Triangulation of Resonance Energy Transfer Distance Measurements[†]

Dipesh A. Patel and Douglas D. Root*

University of North Texas, P.O. Box 305220, Denton, Texas 76203-5220

Received August 16, 2008; Revised Manuscript Received November 17, 2008

ABSTRACT: Cooperative activation of the thin filament is known to be influenced by the tight binding of myosin to actin, but the molecular mechanism underlying this contribution of myosin is not well understood. To better understand the structural relationship of myosin with the regulatory troponin complex, resonance energy transfer measurements were used to map the location of troponin relative to a neighboring myosin bound to actin using atomic models. Using a chicken troponin T isoform that contains a single cysteine near the binding interface between troponins T, I, and C, this uniquely labeled cysteine on troponin was found to be remarkably near loop 3 of myosin. This loop has previously been localized near the actin and myosin interface by chemical cross-linking methods, but its functional contributions have not been established. The implications of this close proximity are examined by molecular modeling, which suggests that only restricted conformations of actomyosin can accommodate the presence of troponin at this location near the cross-bridge. This potential for interaction between troponin and myosin heads that bind near it along the thin filament raises the possibility of models in which direct myosin and troponin interactions may play a role in the regulatory mechanism.

The molecular regulation of striated muscle contraction depends on the interactions of a highly organized macromolecular network of proteins in the thin filament. Troponin (Tn),[1] tropomyosin (Tm), and actin constitute the majority of the thin filament and are initially signaled by the binding of Ca^{2+} (*1*). They bind to an actin filament core formed by an array of actin monomers, and the position of Tm is believed to be influenced by Ca^{2+} and myosin binding (*2, 3*). The head to tail association of Tm dimers forms a cofilament on actin with each Tm dimer binding about seven actin monomers (*4*). Tn, the companion regulatory protein, is a complex of three proteins, TnT, TnI, and TnC (*5*), that binds along the actin filament every seven actin monomers. TnI binds actin in the absence of Ca^{2+}, and a Ca^{2+} transducer segment (switch) of TnI binds the N-terminal of Ca^{2+}-activated TnC (*6*). The binding of TnC to Ca^{2+} enables the contractile response (*7*). TnT contacts Tm, TnI, and TnC (*1, 8, 9*). Ca^{2+} relieves the attachment of the TnI inhibitory segment to actin, which, in turn, releases the Tm to reposition along the thin filament (*4, 10, 11*). Rigor-like binding of myosin to actin has been shown to affect the Tm position on the thin filament and contribute to the cooperative activation of the thin filament, but the sites of communication between myosin and Tn/Tm have not been well characterized (*12, 13*).

Various atomic models have been proposed for the relationship between actin and skeletal myosin, but in these models the Tn and Tm complex has not been included (*14*−*19*). One problem is that the X-ray crystallographic structures upon which these models are based may not represent the true actin-bound conformation form due to the conditions required to prepare protein crystals. A different problem is apparent for electron microscopy-derived structures, which lack the detailed resolution present in crystallographic models but directly examine the actin and myosin complex. In addition, because of the limitations imposed by the inherent structure of the thin filament with Tn bound at every seventh actin monomer, electron microscopy has great difficulty in identifying their positions relative to bound myosin (*11, 20, 21*).

A method that does permit a physiological environment under which proximity relationships between specific sites can be studied is fluorescence resonance energy transfer

[†] We gratefully acknowledge support from the National Institutes of Health, Grant AR44737.

* Corresponding author. E-mail: DROOT@UNT.EDU. Phone: 940-565-2683. Fax: 940-565-4136.

[1] Abbreviations: AlF_4, aluminum fluoride; AmrB, aminorhodamine B; BeF_x, beryllium fluoride; β-me, β-mercaptoethanol; CM, carboxymethyl; CS124, carbostyril 124, 7-amino-4-methyl-2(1*H*)-quinolinone; C-TnT, C-terminal of TnT; DEAE, diethylaminoethyl; DMF, dimethylformamide; DMSO, dimethyl sulfoxide; DTNB, 5,5′-dithiobis(2-nitrobenzoic acid), Ellman's reagent; DTPA, diethylenetriaminepentaacetic acid; DTT, dithiothreitol; ε, molar extinction coefficient; *E*, efficiency of energy transfer; E-64, *trans*-epoxysuccinyl-L-leucylamido(4-guanidino)butane; EDTA, ethylenediaminetetraacetic acid; EGTA, ethylene glycol tetraacetic acid; ELC, essential light chain; Em λ, emission wavelength; F-actin, filamentous actin; FHS, fluorescein-5(6)-carboxamidocaoric-*N*-hydroxysuccinimide; FRET, fluorescence resonance energy transfer; LRET, luminescence resonance energy transfer; MCMM, Monte Carlo molecular mechanics force field; MES, 2-(*N*-morpholino)ethanesulfonic acid; MWCO, molecular weight cutoff; NEM, *N*-ethylmaleimide; OPLS-AA, optimized potential for liquid simulations−all atom force field; PEG, polyethylene glycol; PMSF, phenylmethanesulfonyl fluoride; PRCG, Polak−Ribiere conjugate gradient energy minimization method; *R*, distance between donor and acceptor pair; R_o, critical transfer distance at which *E* is 50%; RLC, regulatory light chain; S1, subfragment 1 of myosin; SDS−PAGE, sodium dodecyl sulfate−polyacrylamide gel electrophoresis; Tm, tropomyosin; TMR, tetramethylrhodamine; 5-TMRIA, tetramethylrhodamine-5-iodoacetamide dihydroiodide; Tn, troponin complex; TnC, troponin C; TnI, troponin I; TnT, troponin T; Tris, tris(hydroxymethyl)-aminomethane.

10.1021/bi801554m CCC: $40.75
Published on Web 12/24/2008

(FRET). This spectroscopy-based technique depends on the distance between a so-called donor and acceptor probe between which energy transfer occurs. In this work, a modified version of this method was used, called luminescence resonance energy transfer (LRET), which employs a lanthanide terbium atom as the donor instead of the conventional dye probes that are prone to larger errors in distance measurements. Typically, two probes in close proximity will yield a higher efficiency of energy transfer (shorter distance) than a pair farther away (longer distance), ultimately yielding distance values over a 1−10 nm range. The distances reported in atomic models of actin and actomyosin (*2, 22*−*24*) correlate well with most of the corresponding distances measured by FRET. In particular, FRET has revealed the distance between specific sites on actin/TnT (*25*), actin/Tn (*26*), and actin/Tm (*27, 28*), but measurements between other protein pairs are lacking.

In the present study, a multisite LRET approach is used to map the position of a site on TnT that is juxtaposed to the interface between the TnI, TnC, and TnT components of Tn based on the crystallographic structures (*29, 30*). Site-specific labeling of TnT by a Tb^{3+} chelate is accomplished by means of a single cysteine (Cys263) present near the C-terminal region (C-TnT) of a naturally occurring chicken isoform of TnT (*31*). Distance measurements are made from the donor probe on TnT to three different S1 acceptor sites including the nucleotide site, Cys707, and Lys553. Since these distances each share a common point of reference (donor), using knowledge on the location of each acceptor site on S1 via current X-ray crystallographic models provides means to map the location of C-TnT into the atomic models by satisfying the distance requirements between each donor−acceptor pair. In addition, both the prepowerstroke and postpowerstroke conformations of myosin docked onto atomic models of the actin filament are analyzed to assess the most likely conformations of the proteins. Consequently, the mapped region of C-TnT indicates potential interactions with the proteins present in the model (S1 and actin) based on its proximity, most notably with myosin loop 3. These results suggest that the postpowerstroke state is inhibited by the adjacent Tn complex, thus suggesting that these myosin molecules do not participate in filament shortening (force production). The physiological and regulatory implications in muscle contraction are discussed in further detail.

MATERIALS AND METHODS

Protein Preparation. Rabbit psoas muscle myosin was prepared by the method of Godfrey and Harrington (*32*), from which myosin S1 was prepared using papain or α-chymotrypsin and purified according to Weeds and Pope (*33*). Rabbit skeletal actin was prepared by the method of Spudich and Watt (*34*). Chicken breast TnT was purified as previously described by Zhang et al. (*35*) because its unique cysteine residue allowed for specific labeling with a Tb^{3+} atom chelate, while Tm was purified from actin acetone powder by the method of Smillie (*36*). Isolation of Tn subunits and the subsequent reconstitution of rabbit Tm, TnI, and TnC and labeled chicken TnT were carried out by the method of Potter (*37*). RLC was isolated by dissociation from rabbit skeletal myosin as described by Xu and Root (*38*). Protein concentrations were determined using the following molar extinction coefficients at 280 nm, ε_{280nm} (M^{-1} cm^{-1}): myosin dimer, 264000; myosin S1, 82500; actin, 46200 (ε_{290} = 26460); actin 7-mer, 323400; TnT (denatured), 26000; TnT, 12000; TnI (denatured), 8500; TnC (denatured), 3300; Tm (denatured) dimer, 15840; Tn complex, 32400; Tn−Tm complex, 47340; RLC, 12000.

Synthesis of Tb^{3+} Chelate and TnT Labeling. The maleimide-modified CS124 Tb^{3+} chelate was synthesized following a protocol previously described by Root et al. (*15*) but modified by using the CS124 antenna. The concentration of CS124 was determined from a molar extinction coefficient, ε_{337} = 12000 M^{-1} cm^{-1}.

Myosin S1 Labeling. Three labels, (A) Cy5-ATP, (B) 5-TMRIA "single isomer" (Molecular Probes), and (C) FHS (Sigma Chemical Co., St. Louis, MO), were used to label the myosin head domain in independent experiments. Cy5-ATP was synthesized similarly to Cy3-ATP as previously described by Xu and Root (*38*). Cy5-ATP ε_{646} = 250000 $M^{-1}cm^{-1}$; Em λ = 670 nm. 5-TMRIA was prepared based on the method described by Root et al. (*39*) where the fluorophore was dissolved in 1 mL of DMF, added to S1 in a 1:1 molar ratio, and incubated for 30 min. The reaction was terminated by addition of a 10-fold molar excess of DTT and dialyzed in 0.04 M KCl and 10 mM imidazole, pH 7, at 4 °C (TMR ε_{543} = 87000 M^{-1} cm^{-1}; Em λ = 567 nm). S1 was incubated with FHS as described by Bertrand et al. (*40*), where glycine was used to quench the reaction (FHS ε_{495} = 75000 M^{-1} cm^{-1}; Em λ = 520 nm). Purified RLC was labeled with AmrB-DTPA via a method previously described by Root (*41*), but with AmrB used instead of cytosine (AmrB ε_{550} = 110000 M^{-1} cm^{-1}; Em λ = 568 nm). Labeled RLC was then exchanged back into S1 by the method of Root et al. (*39*). Absorbance spectra show ∼50%, 7%, and 11% efficiency of labeling (not shown) of TMR, FHS, and AmrB, respectively, and an exchange efficiency of RLC-AmrB with endogenous papain S1 RLC of ∼5%.

Exchange of Labeled TnT with Endogenous TnT in Myofibrils. Rabbit myofibrils derived from the method of Godfrey and Harrington (*34*) were stored in 50% glycerol at −20 °C and then prepared for TnT exchange similarly to the method of Shiraishi et al. (*42*). Then 0.5 mL of 0.1 mg/mL chicken TnT-chelate was added to 0.5 mL of myofibril to a final myofibril concentration of 50 μg/mL and gently agitated for 60 min at 25 °C. Endogenous TnT, TnI, and TnC was removed by centrifugation The myofibrils were dialyzed in 50 mM KCl, 10 mM imidazole, and 1 mM $NaHCO_3$ for 6 h before TnI and TnC were added in equimolar amounts with respect to the initial amount of chicken TnT-chelate added and incubated overnight at 4 °C. $MgCl_2$ was added to 1 mM before the sample was split into two tubes, with one containing $CaCl_2$ to 0.1 mM and the other with EGTA to 0.5 mM. A control sample containing unlabeled chicken TnT was also prepared.

Preparative Equipment. Myosin S1 was stored at 4 °C and used within 2 weeks to ensure its integrity. All other proteins were flash frozen, stored at −70 °C, and prepared as required. The Bio-Rad Mini-PROTEAN II system was used with 12% or 15% SDS−PAGE, which confirmed the isolation, purification, and labeling of all proteins. Column chromatography was carried out using a Pharmacia Biotech FPLC system (controller LCC-501 plus, pump P-500) with 254 nm UV detector and conductivity monitor to purify all

proteins. Centrifugation was performed using a Sorvall RC-5B DuPont centrifuge (GSA rotors) and a Beckman Tabletop ultracentrifuge (TLA rotors).

LRET Data Collection. The reconstituted thin filament sample was one with 0.1 mM $CaCl_2$ and the other with 0.5 mM EGTA. When measuring LRET, acceptor-labeled S1 was added to the reconstituted thin filament sample in a 1:1 ratio with respect to the molar concentration of actin monomer (~1 μM). Up to four sequential emission scans and fluorescence donor lifetime measurements were obtained in the reconstituted contractile system or myofibrils: (1) in the presence of Tb^{3+} donor only (TnT-chelate), (2) after addition of acceptor-labeled S1, (3) after addition of ADP (or hydrolysis of Cy5-ATP to Cy5-ADP), and (4) where permitted, addition of phosphate analogue (beryllium fluoride, BeF_x, and aluminum fluoride, AlF_4, in independent experiments). The distance between probes was measured in up to three myosin/S1 states: rigor (no nucleotide), postpowerstroke, and prepowerstroke. Cy5-ATP was added to S1 and myofibril at 0.5 μM and incubated for 5 min to allow for hydrolysis to the Cy5-ADP form, after which measurements were made. Each day, fresh stock solutions of BeF_x and AlF_4 were prepared by mixing 1 mM atomic BeF_x or $AlCl_3$ with 10 mM NaF. Phosphate analogues, at 0.1 mM Be^{3+} or Al^{3+} and 1 mM F^-, and ADP were incubated for 15 min before data acquisition.

LRET Data Analysis. All decay times at the donor Em λ = 545 nm were fit to a double exponential function, $F(x) = a^{-x/b} + c + d^{-x/e}$, except for the donor only curve, which was fit to a single exponential function, $F(x) = a^{-x/b} + c$. Similarly, all decay times at the acceptor emission wavelengths were fit to the single exponential equation, except for the donor only curve that was fit to a value of 0 ($F(x) = c$). These different donor times were used to calculate the efficiency of resonance energy transfer, E, in the tested myosin states (eq 1).

$$E = 1 - (T_{da}/T_d) \quad (1)$$

Here, the long-lived apparent lifetime of the acceptor (T_{da}) in the presence of Tb^{3+} is equal to that of the quenched Tb^{3+}. Thus, E is calculated by comparison to the lifetime of the donor in the absence of acceptor, T_d. Next, J, the spectral overlap integral (eq 2), followed by R_o, the critical transfer distance at which energy transfer is 50% (eq 3), was determined.

$$J = \sum[\Phi_D(\lambda)\varepsilon_A(\lambda)\lambda^4\Delta\lambda]/\sum[\Phi_D(\lambda)\Delta\lambda] \quad (2)$$

$$R_o = [(8.785\times10^{-11})Q_D\eta^{-4}\kappa^2 J]^{1/6} \quad (3)$$

$\Phi_D(\lambda)$ is the relative emission of the donor at a certain wavelength, $\varepsilon_A(\lambda)$ is the extinction coefficient of the acceptor at the same wavelength, and $\Delta\lambda$ is the interval between wavelengths (1 nm). Q_D is the quantum yield of the donor (T_{da}/T_d), η is the refractive index of the protein medium (1.4), κ^2 is the orientation factor assumed to be $^2/_3$, and J is the overlap integral that depends on the chosen acceptor. Finally, R, the distance separation (nm) between the donor and acceptor probe in each tested condition, was obtained after rearranging eq 4.

$$E = R_o^6/(R_o^6 + R^6) \qquad R = R_o[(1 - E) - 1]^{1/6} \quad (4)$$

Triangulation of C-TnT in Actomyosin Atomic Models. All three S1 labels (Cy5-ATP, TMR, and FHS) allowed for distance measurements to be made to the donor probe attached to C-TnT in the postpowerstroke state. Average values obtained in the presence of Ca^{2+} were used to map the position of C-TnT since those measured in low Ca^{2+} conditions were not significantly different. Since the fixed location of each acceptor site on S1 was known and their relative distances from the donor probe using X-ray crystallographic models, it was possible to map the location of C-TnT into the atomic models. PDB coordinates of the actomyosin atomic model were used to incorporate the x, y, z coordinates of C-TnT. Here, the coordinates were calculated with respect to the S atom of Cys707, the terminal side chain N atom of Lys553, and the C^α atom of Trp131, corresponding to TMR, FHS, and Cy5-ATP, respectively. Trp131 was previously used to represent the ATPase site by Xu and Root (*38*) when a very similar probe, Cy3-ATP, was used. The two possible solutions, which reside about a plane of symmetry, were resolved using an acceptor probe, AmrB. The position of C-TnT was observed in three different actomyosin atomic models referred to here as model 1, model 2, and model 3, each of which was derived by different means. All models employed crystal structures of actin (*23, 43*) and skeletal chicken myosin (*44*) in the rigor state. RasMol software was used to observe the structures. Model 1 is based on the objective docking of S1 with actin guided by cryoelectron microscopy density maps (*22*) accomplished by Rayment et al. (*24*). Model 2 is also based on electron microscopy maps; however, docking of S1 onto F-actin (*2*) was done computationally by Mendelson and Morris (*45*). The coordinates for this model represent only C^α atoms, so the distance from C-TnT to the C^α of Cys707 and Lys553 was calculated from model 1 and transferred to model 2. This correction factor is essential to determine the most accurate position of C-TnT relative to the C^α atoms of the three myosin labeling sites. Model 3 was determined solely via computational docking of S1 (*44*) and F-actin (*2*) by Root (*46*).

Conformational Search of Tb^{3+} Chelate Bound to TnT. Maestro modeling software (Schrödinger, Inc.) was used to construct Tb-DTPA-CS124-NEM according to Getz et al. (*47*) and to mutate the solved crystal structure of human cardiac Tn (*30*). Here, the appropriate chicken breast TnT residues including an exclusive Cys263, the point of chelate attachment, were substituted to be included in the computational simulations. Conformational searches of the chelate bound to Cys263 were performed using (1) the OPLS-AA force field with water at normal distance, (2) 0.25 nm distance constraints between the three closest oxygen atoms of the chelate and Tb^{3+} ion, (3) the chelate and TnT interface residues with surrounding atoms up to a 0.3 nm radius from Cys263 and allowing them to freely move (Figure 1), (4) energy minimization algorithms via the PRCG method at 1000 iterations, and (5) conformational searches via the Mixed MCMM/LowMode method with automatic setup of bond rotations and all default settings. After each round of 1000-step iterations, the lowest energy structure was used as the starting structure of the next iteration until no change in conformation and energy was observed.

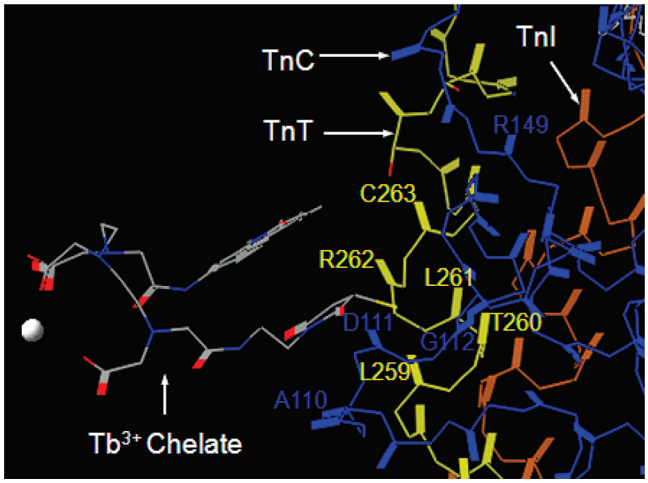

FIGURE 1: Tn residues near the chelate binding interface. Some TnC residues, A110−G112 and G148−R149 (blue), and TnT residues L259−C263 (yellow) were allowed to freely move during conformational searches due to their close proximity to the Tb^{3+} chelate. For example, L259, R262, and C263 are located within 0.5 nm. Amino acid numbers are located near the carbonyl group (thick lines) of their respective residues.

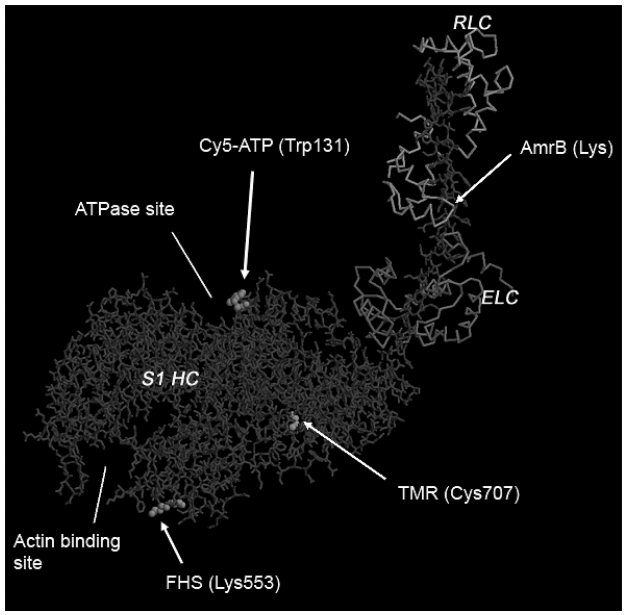

FIGURE 2: Atomic model of labeled myosin S1. Myosin S1 heavy chain (HC) residues that react with or are located near acceptor fluorophores, Cy5-ATP, TMR, and FHS, are shown as space-filled structures located at Trp131, Cys707, and Lys553, respectively. AmrB labels lysine(s) at the N-terminal of the RLC.

RESULTS

Myosin S1 and TnT Labeling. Four different sites of S1 were labeled with acceptor fluorophores in separate experiments (Figure 2), and SDS−PAGE confirmed the attachment of TMR and FHS labels to the heavy chain and AmrB to the RLC (not shown). These labeling methods have previously been characterized as described in Materials and Methods. The absence of the N-terminal region of RLC as observed in X-ray crystallographic structures implies a highly flexible and mobile region that is consequently characterized by weak electron density (*44*). Therefore, also implied by Xu and Root (*38*) even knowledge on the specific N-terminal location of AmrB-labeled lysine(s) would not be sufficient in calculating an accurate distance value. Since these LRET-derived distance measurements are consistent with the atomic models, it supports that fluorophore labeling of S1/RLC and TnT did not significantly alter the structure and function of the contractile system. In addition, previous studies on labeling the N-terminal of the RLC and Cy3-ATP labeling of the myosin ATPase site have shown no adverse functional effects as revealed by in vitro motility, ATPase activity, and fiber assays (*38, 48, 49*). We therefore expect Cy5-ATP, having the same structure as Cy3-ATP in addition to two more carbon atoms bridging the aromatic cyanine (Cy) groups, to behave similarly.

Previously, the functional effects of labeled chicken TnT on its exclusive cysteine residue using three different fluorophores were observed to maintain similar calcium-activated myofibrillar ATPase activity compared with controls (*31, 35, 50*). This strongly supports that our experimental system employing TnT from chicken breast muscle in addition to other contractile components from rabbit is adequate to mimic a fully functional skeletal contractile system. Our conformational searches also supporting these fluorescence lifetime data in the presence of TnT-chelate showed decay times typically greater than 1 ms confirming Tb^{3+} binding to the chelate versus faster lifetimes that otherwise indicated unbound Tb^{3+} (not shown). This was observed both for S1 and myofibril experiments.

LRET Measurements between C-TnT and Myosin S1. The emission scans of Tb^{3+}-labeled chicken TnT in the reconstituted regulated rabbit actin filament in the presence of acceptor-labeled S1 are summarized in Figure 3. Energy transfer between the Tb^{3+} donor and each acceptor probe (Cy5-ATP, TMR, FHS, and AmrB) was observed at the appropriate emission wavelength where only the acceptor emits a signal upon addition of the acceptor-labeled S1 to the donor. For example, Cy5-ATP shows an increase in signal (sensitized emission) at 670 nm in the presence of donor (Figure 3). Donor quenching is also indicative of energy transfer in the presence of acceptor; however, our emission scans are normalized to 545 nm (maximum donor emission) and thus do not show this. Energy transfer can also be observed by measuring the fluorescence lifetime decay of the donor in the presence of acceptor at the wavelength where only the acceptor probe emits signal (Figure 4). Typically, the donor decay lifetime in the presence of acceptor was fast relative to that in its absence, suggesting the donor was in close proximity for energy to be transferred to the acceptor. These lifetimes were used to calculate the efficiency of energy transfer (E) between each acceptor (A) and donor pair and distance measurements in nm (R) from eqs 1 and 4, respectively. The results are presented in Table 1 in the presence (Y, yes) and absence (N, no) of calcium. The table also indicates which phosphate analogue (PA) used to induce the prepowerstroke state and R_o values, defined as the distance at which E is 50%.

As previously described by Root et al. (*15*) and Root and Reisler (*51*), FRET measurements involving TMR-labeled S1 Cys707 were made only in the rigor and postpowerstroke state (+ADP), due to the modified Cys707 influencing pre/postpowerstroke state transitions. Therefore, LRET was not measured in the presence of phosphate analogues in TMR-labeled S1 experiments. Maruta et al. (*52*) and Werber et al. (*53*) have previously shown that, in the presence of S1·MgADP and varying AlF_4 or BeF_x concentrations, the

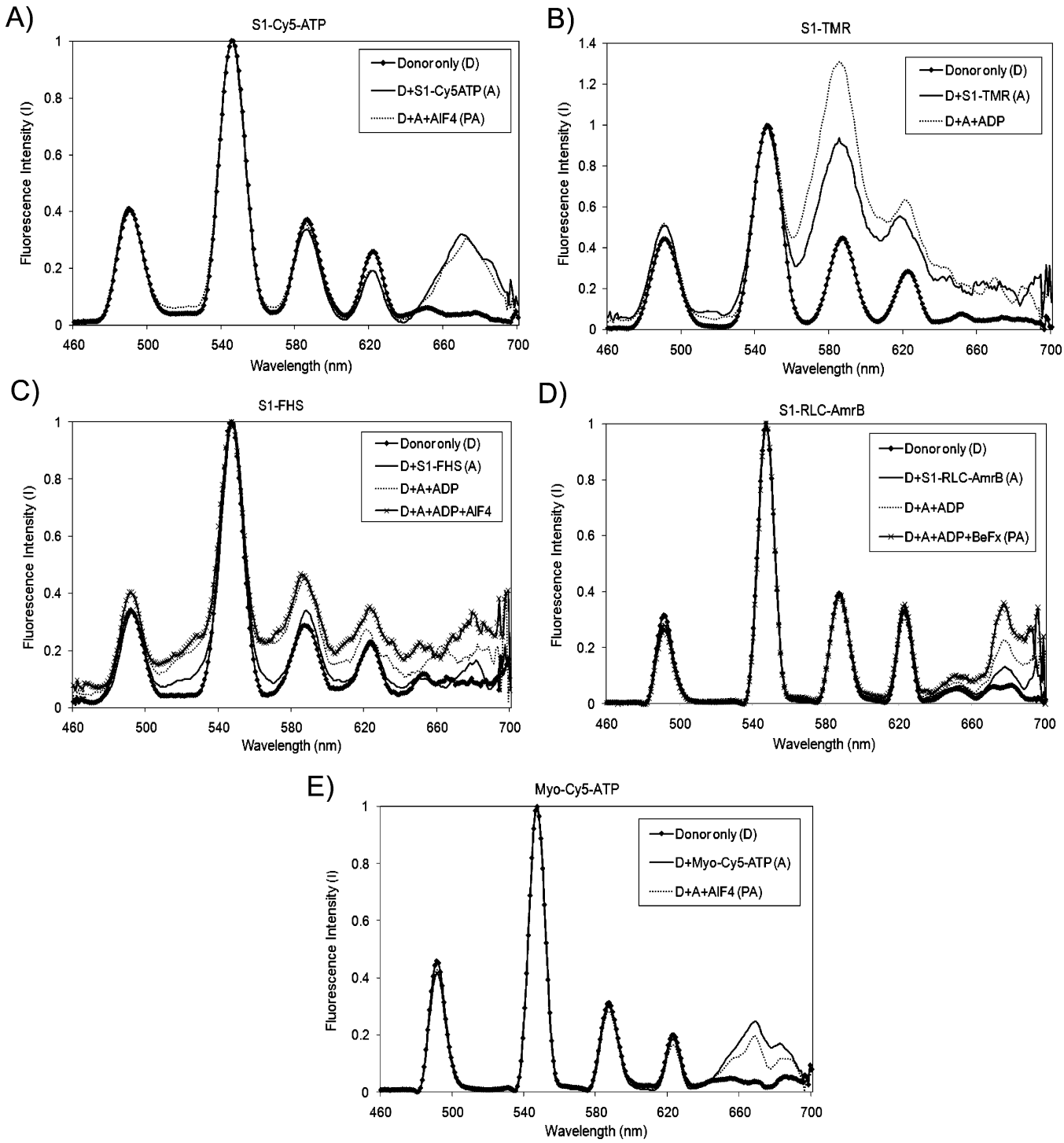

FIGURE 3: Emission spectra of Tb^{3+}-labeled chicken TnT. The signal was measured in the reconstituted thin filament and in the presence of S1 labeled with (A) Cy5-ATP, (B) TMR, (C) FHS, (D) RLC-AmrB, and (E) same as (A) but in myofibrils (Myo). Conditions tested include the control, i.e., in the presence of Tb^{3+} donor only (D), followed by addition of acceptor (A), ADP, and phosphate analogue, either BeF_x or AlF_4. Each trace has been normalized at 545 nm, the maximum emission peak of Tb^{3+}.

formation of the S1·MgADP·AlF_4 or S1·MgADP·BeF_x complex inhibits S1 ATPase activity. This type of behavior indicates the formation of stable S1−phosphate analogue complexes. It is clear that the stable complex is achieved in our LRET experiments since a higher ratio of phosphate analogue to S1 was used under similar conditions compared to Werber et al. (*53*). It has also been observed that these phosphate analogues in the presence of ADP cause the actomyosin complex to dissociate, yet favor a transient weak binding state that mimics the prepowerstroke state (*38, 52, 54*). Xu and Root (*38*) have previously shown that, as a control, the lifetime of free Tb^{3+}-bound chelate in the presence of phosphate analogue did not significantly change, thus eliminating the possibility of the phosphate analogues quenching the donor signal.

In the present study, addition of the first acceptor probe, Cy5-ATP, to S1 causes it to bind to the ATPase site, which then rapidly hydrolyzes the nucleotide to the diphosphate form (Cy5-ADP) inducing the postpowerstroke state. Moss and Trentham (*55*) have approximated the binding constant

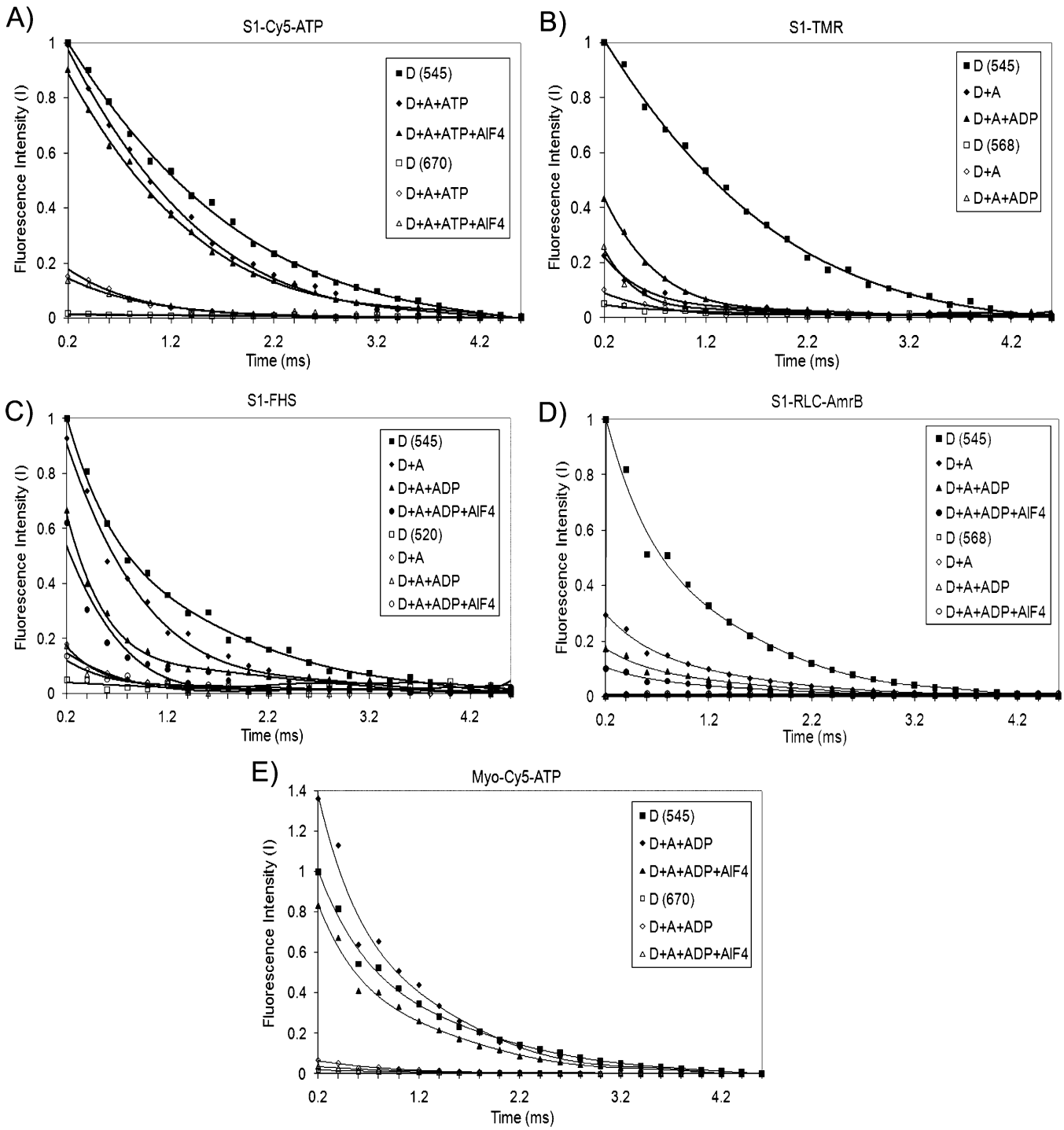

FIGURE 4: Fluorescence lifetime decay of Tb^{3+}-labeled chicken TnT. Myosin S1 labeled with (A) Cy5-ATP, (B) TMR, (C) FHS, (D) RLC-AmrB, and (E) same as (A) but in myofibrils (Myo). Conditions tested correspond to those described in Figure 3. Measurements were obtained at the emission maximum wavelength (545 nm) of the Tb^{3+} donor (D), indicated by the solid symbols, and the specific emission wavelength of the acceptor (A), indicated by the open symbols. The emission wavelength for each acceptor is also indicated in parentheses.

of ADP to heavy meromyosin to be about 1.3×10^6 M^{-1}, supporting that a high fraction of Cy5-nucleotide is bound at the S1 nucleotide site in our experiments. An even larger binding constant is expected in the presence of phosphate analogues which can trap the nucleotide. Xu and Root (*38*) showed there is no significant interference from diffusion-enhanced quenching from free Cy3-ATP as the acceptor concentration approaches half of the donor-labeled myosin concentration. Again, similar behavior is expected from Cy5-ATP. In our experiments, a Cy5-ATP:S1 ratio of 1:14 was used, thus likely eliminating diffusion-enhanced energy transfer. Data support that calcium causes only a slight change in the efficiency of resonance energy transfer in either the pre- (phosphate analogue) or post- (ADP) powerstroke state (Table 1). Representative results (not shown) of the donor only lifetime (ms) are 1.34 ± 0.14 and 1.77 ± 0.1 in the presence and absence of calcium, respectively. Then, after addition of Cy5-ATP and subsequent hydrolysis to the ADP form, there is a decrease to 0.65 ± 0.04 (+Ca) and 0.70 ± 0.10 (−Ca), indicative of energy transfer. Finally, addition

Table 1: LRET-Derived Distances between C-TnT and Myosin

						rigor (no nucleotide)		postpowerstroke (ADP)		prepowerstroke (ADP + PA)	
	A	site	Ca	PA	R_o	*E*	*R*	*E*	*R*	*E*	*R*
S1	Cy5-ATP	ATP	Y	AlF_4	4.84 ± 0.09	NA	NA	0.48 ± 0.05	4.90 ± 0.10	0.43 ± 0.06	5.09 ± 0.18
				BeF_x	4.88 ± 0.06			0.53 ± 0.07	4.78 ± 0.17	0.51 ± 0.07	4.85 ± 0.17
			N	AlF_4	5.11 ± 0.03			0.60 ± 0.06	4.79 ± 0.25	0.55 ± 0.05	4.93 ± 0.18
				BeF_x	5.08 ± 0.05			0.61 ± 0.06	4.73 ± 0.16	0.56 ± 0.05	4.90 ± 0.12
	FHS	Lys553	Y	AlF_4	4.02 ± 0.02	0.73 ± 0.04	3.42 ± 0.09	0.72 ± 0.04	3.44 ± 0.11	0.76 ± 0.05	3.33 ± 0.14
				BeF_x	4.04 ± 0.02	0.76 ± 0.05	3.35 ± 0.15	0.75 ± 0.07	3.36 ± 0.21	0.73 ± 0.06	3.43 ± 0.16
			N	AlF_4	4.01 ± 0.05	0.74 ± 0.04	3.35 ± 0.07	0.75 ± 0.02	3.33 ± 0.05	0.76 ± 0.03	3.30 ± 0.04
				BeF_x	4.02 ± 0.04	0.76 ± 0.03	3.31 ± 0.11	0.73 ± 0.03	3.40 ± 0.08	0.74 ± 0.01	3.38 ± 0.06
	TMR	Cys707	Y	NA	5.26 ± 0.03	0.75 ± 0.03	4.37 ± 0.15	0.72 ± 0.02	4.49 ± 0.07	NA	NA
			N	NA	5.24 ± 0.02	0.78 ± 0.04	4.23 ± 0.16	0.67 ± 0.01	4.65 ± 0.06		
	AmrB	RLC	Y	BeF_x	5.20 ± 0.01	0.01 ± 0.01	≥11.6 ± 0.01	0.02 ± 0.01	≥9.97 ± 0.36	0.02 ± 0.01	≥9.86 ± 0.80
myofibril	set 1, Cy5-ATP	ATP	Y	AlF_4	5.40 ± 0.22	NA	NA	0.41 ± 0.03	5.74 ± 0.32	0.47 ± 0.10	5.50 ± 0.31
				BeF_x	5.52 ± 0.13			0.34 ± 0.04	6.17 ± 0.31	0.35 ± 0.07	6.15 ± 0.17
			N	AlF_4	5.81 ± 0.13			0.59 ± 0.03	5.48 ± 0.08	0.60 ± 0.02	5.44 ± 0.17
				BeF_x	5.74 ± 0.16			0.44 ± 0.10	5.97 ± 0.27	0.50 ± 0.09	5.76 ± 0.31
	set 2, Cy5-ATP	ATP	Y	AlF_4	5.65 ± 0.08	NA	NA	0.62 ± 0.07	5.20 ± 0.22	0.63 ± 0.03	5.15 ± 0.02
				BeF_x	5.41 ± 0.05			0.50 ± 0.01	5.41 ± 0.08	0.53 ± 0.05	5.29 ± 0.11
			N	AlF_4	5.73 ± 0.16			0.63 ± 0.01	5.23 ± 0.11	0.64 ± 0.02	5.19 ± 0.22
				BeF_x	5.64 ± 0.12			0.56 ± 0.06	5.42 ± 0.22	0.61 ± 0.03	5.25 ± 0.20

of AlF_4 or BeF_x yielded decay times of 0.77 ± 0.10 (+Ca) and 0.72 ± 0.03 (−Ca), respectively. This observation suggests the binding of calcium to the N-domain of TnC does not cause a shift by more than about 0.2 nm of the C-terminal of TnT away from the myosin ATPase site. The comparable efficiency of energy transfer in both the presence and absence of calcium indicates that the prepowerstroke state of S1 forms irrespective of calcium levels. Distance values range from about 4.7 to 5.1 nm (Table 1).

The second acceptor probe, TMR, was used to label Cys707 (SH1), which resides near the myosin head/neck junction (converter region) and is the most reactive labeling site on myosin (*39*). While the consequences of *complete* S1-Cys707 modification include strong inhibition of K^+ (EDTA) ATPase activity and a decrease in acto-S1 ATPase activity, partial modification of this group by Root et al. (*39*) shows the acto-S1 ATPase activity to decrease proportionally according to the level of SH1 labeling. In our experiments, since ∼50% labeling efficiency was calculated by absorbance spectra, a high level of acto-S1 ATPase activity was assumed to be maintained as in accordance with Root et al. (*39*). Note though, because different effects of labeling SH1 on myosin have been observed, the true form of the cross-bridge cycle is open to debate, and so data with spectroscopic probes on this site must be interpreted carefully (*39*). Interestingly, Greene and Eisenberg (*56*) have shown similar S1 binding results between iodoacetamide-labeled SH1 S1 and unmodified S1 in actin binding assays. In the present study, since no nucleotide-based fluorophore was used as the acceptor probe, the myosin rigor state was monitored before the postpowerstroke state (addition of ADP). Results indicate the distance between probes in the rigor state is maintained (4.3 ± 0.15 nm) irrespective of calcium levels. Activated Tn also appears to maintain the position of TMR/C-TnT during the transition from the rigor to the postpowerstroke state. This does not, however, rule out the possibility of a conformational change because a similar distance can still be maintained even after an apparent structural shift. This correlates with donor only lifetimes (ms) averaging 1.56 ± 0.06 regardless of calcium levels and then after addition of S1-TMR followed by ADP yields similar times of 0.42 ± 0.04 and 0.34 ± 0.05, respectively. A small but significant increase in distance (0.2−0.64 nm) is observed in the absence of calcium during the rigor-to-postpowerstroke state transition, along with 0.04−0.3 nm increase in distance in the absence of calcium observed in the postpowerstroke state (Table 1).

The third acceptor probe, FHS, attaches to Lys553 located in the helix−turn−helix motif (residues 516−558) of myosin and is an important site to monitor the binding characteristics of S1 to actin. This site is near the primary actin-binding site thought to contribute to the tight, hydrophobic interaction of S1 with subdomain 1 of actin (*24*). Cosedimentation experiments reveal no disruption of the rigor acto−S1 interaction when Lys553 is labeled, and this does not drastically affect the biological activity of S1 (*40*). LRET data were collected in three myosin states: rigor, prepowerstroke, and postpowerstroke. The distance between FHS and C-TnT does not change significantly during the transition from rigor to the post/prepowerstroke states or even between the post/prepowerstroke states (∼3.4 nm). Also, calcium appears to have no appreciable influence on the distance between probes, and low levels do not appear to prevent formation of the prepowerstroke state due to the presence of energy transfer (Table 1). Here, donor only lifetimes (ms) average 1.18 ± 0.05, and all tested S1 states after addition of S1-FHS average 0.30 ± 0.04. Collectively, these findings suggest FHS may reside at a fulcrum region about which the S1 head pivots when transitioning from the pre- to the postpowerstroke state and on to the rigor state. Consequently, a relatively constant distance with respect to C-TnT is maintained throughout these S1 states, which is also consistent with the known interaction between Lys553 and actin (*24*).

Having determined the distance between each donor−acceptor pair in the S1 postpowerstroke state, while knowing the fixed location of each acceptor on S1, the coordinates corresponding to the location of C-TnT (donor) were solved using the coordinates from current actomyosin atomic models. Since two solutions for C-TnT were identified while satisfying the distance requirements of the donor probe from the known location of each acceptor probe, the RLC was chosen as an additional acceptor site to determine the most likely location. AmrB was used to label the N-terminal region

of RLC, although it was unclear which RLC N-terminal lysine(s) is (are) labeled. This site is referred to as RLC-Lys in Figure 1. According to actomyosin atomic models, both potential locations of C-TnT were located about 10−12 nm away from the N-terminal region of RLC, close to the upper range of the detection limit of LRET. However, since minimal resonance energy transfer (1−2%) was observed (Figures 3D and 4D, Table 1), this indicated that one site, located nearer the actin filament, was slightly closer to RLC and thus the more likely location for C-TnT. Little change was detected between probes on RLC and C-TnT during the transition from the rigor to the pre/postpowerstroke state due to the weak signal and relatively long distance (10−12 nm).

LRET Measurements in Myofibrils. To compare the LRET measurements derived from myosin S1−Cy5-ATP and reconstituted thin filament proteins, Tb^{3+}-labeled chicken TnT was exchanged into rabbit skeletal myofibrils. This represents the native state of thick and thin filaments in the presence of other structural and contractile elements and serves as a reference to compare the analogous S1 data. Only Cy5-ATP was added directly to myofibrils because of its high affinity and specificity to the myosin ATPase site. The other acceptor fluorophores used in S1 experiments were not employed in the myofibril study because they cannot be attached specifically to the target protein due of the presence of all the other muscle proteins in the myofibril. Actin is already saturated with unlabeled nucleotide which exchanges only very slowly (*57*), and other extraneously bound CY5-ATP would not likely be in close proximity to Tn and play a role in the diffusion-enhanced resonance energy transfer. This is also supported by calculated distance values in all tested conditions being about 1 nm larger in myofibrils. If Cy5-ATP was bound closer to the donor-labeled Tn in myofibrils, then a distance smaller than the reported 5−6 nm (Table 1) would have been observed. Note that two sets of data shown in Table 1 both show no significant difference in distance values either in the pre- or postpowerstroke state. A slightly larger mean distance measurement in set 1 may be due to the myofibril preparation; however, it is evident from set 2 that the distance values are in close agreement as those observed in the analogous S1 measurements. This supports the use of reconstituted contractile proteins as an appropriate model system. Here, a donor only lifetime (ms) is about 1.42 ± 0.05 in both the presence and absence of calcium. Then, after addition of Cy5-ATP and subsequent hydrolysis to the ADP form, there is a decrease to 0.85 ± 0.05 (+Ca) and 0.57 ± 0.05 (−Ca), indicative of energy transfer. Finally, addition of AlF_4 or BeF_x yielded decay times of 0.59 ± 0.06 (+Ca) and 0.53 ± 0.05 (−Ca), respectively.

Conformational Prediction of Tb^{3+} Chelate. The interactions of TnT with TnI and TnC have previously been demonstrated at atomic resolution (*29, 30*). Chicken breast TnT contains a single cysteine residue, the substitution of which in a current model of Tn (*30*) places it near the interface between TnT, TnI, and TnC. This advantageous position was used to monitor structural changes in C-TnT or even motions in nearby TnI and TnC that could otherwise influence the position of C-TnT. Minor structural fluctuations of Tn residues surrounding the chelate attached to TnT suggest the label does not alter the function of the protein complex. Conformational searches suggested the likely

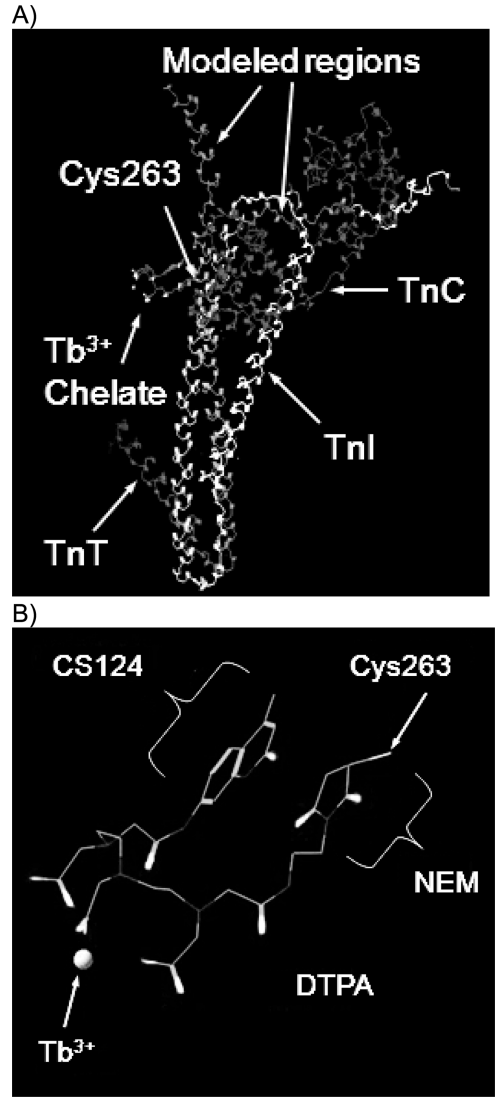

FIGURE 5: Lowest energy structure of the Tb^{3+} chelate. (A) A ribbon diagram shows the conformation of Tb^{3+}-DTPA-CS124-NEM attached to Cys263 of TnT complexed with TnI and TnC (*30*). The complex as shown is about 7.5 nm horizontal and 10 nm vertical. (B) Conformation of the Tb^{3+} chelate at its lowest energy attached to TnT (not shown). The Tb^{3+} atom (white sphere) is coordinated by the closest three carbonyl oxygen atoms from DTPA and the point of attachment to TnT is shown at Cys263 via the *N*-ethylmaleimide moiety (NEM). CS124 serves as an antenna to allow for more efficient Tb^{3+} excitation.

structure of the chelate protrudes away from the Tn complex and toward the solvent, thus minimizing the possibility of interference with normal Tn function (Figure 5A). The chelate is positioned close to the surface of TnT, assuming a relatively compact structure with the CS124 antenna group located <1 nm from the NEM group attached to Cys263 (Figure 5B). This places the Tb^{3+} atom about 1.5 nm from the sulfur (S) atom of TnT Cys263, a value lower in resolution than the X-ray crystallographic structure of Tn (0.33 nm) and so rendering the location of Tb^{3+} on the atomic model highly precise. However, a significant change in the structural relationship of C-TnT as observed in the acto-myosin atomic models is not expected, because the calculated LRET distance, for example, between RLC and TnT, correlates well with the distance measured in the model (∼12 nm).

DISCUSSION

TnT is one of the components along with TnI and TnC in striated muscle that comprises the Tn complex and, in conjunction with Tm, functions to regulate muscle contraction in response to calcium. In particular, the C-terminal region of TnT plays an important role in the transmission of structural changes in the thin filament regulatory proteins initiated by calcium binding to TnC to allow productive interactions between actin and myosin (*29, 30*). While a variety of models have proposed the structural relationship between Tn and actin, the high resolution placement of Tn has proven to be problematic for methods including crystallography, NMR, and electron microscopy. In addition, the location of Tn on actin is not well characterized in the presence of myosin, thus an alternative technique called LRET was used to establish the specific location of C-TnT on the actin filament in the presence of Tm and myosin.

In this study, LRET was measured in the reconstituted thin filament between Tb^{3+}-labeled C-TnT and independently labeled sites on S1 that included the ATP site, actin binding site, converter region, and N-terminal region of RLC. The appearance of LRET even at low calcium levels indicates S1 can still bind to actin within close proximity to Tn for energy transfer to occur. This is consistent with previous findings that support formation of the prepowerstroke state of weakly bound state under similar calcium conditions (*56, 58, 59*). There is no significant change in distance values even when calcium activates Tn, supporting no change in the location of C-TnT with respect to the labeled S1. More specifically, actomyosin atomic models remarkably place C-TnT between loop 3 of S1 and actin helix 91−100 of the adjacent monomer and nearest actin helix 350−358 of the S1-binding monomer, landmarks which have previously been suggested to play a role in S1 strong binding to actin. These models propose C-TnT could hinder this interaction, while favoring direct interactions with S1 and actin, which may impact the regulatory mechanism. This determined position of C-TnT may differ from that in the absence of bound S1 due to the interactions between myosin and Tn; therefore, it is likely to be the most common location for C-TnT during active muscle contraction.

Mapping C-TnT in Actomyosin Atomic Models. Three atomic models previously generated by different S1 docking methods were used to observe the relationship between S1 and the actin filament in the rigor state together with the newly mapped position of C-TnT generated in the postpowerstroke state by LRET. The use of postpowerstroke measurements in the S1 rigor atomic models was valid since the general orientation of the S1 lever arm is similar in both states. The first model (model 1) was determined by the objective docking of S1 on F-actin using electron microscopy density maps, where the bulges observed on the actin filament hinted the general location of the S1 head (*24*). This model is presented in Figure 6, which illustrates the location of C-TnT with respect to S1 and the actin filament. Here, it is apparent that the S1 conformation does not accommodate for the Tn complex due to the implied steric clash between the light chains/lever arm of S1 and Tn. The proposed location of C-TnT using two other actomyosin atomic models from Mendelson and Morris (*45*) and Root (*46*) (designated as model 2 and model 3, respectively) also reveals the same outcome (not shown). Note that the orientation of the Tn complex is arbitrary, while keeping the known location of C-TnT fixed, since it was not possible for Tn to "fit" adjacent to S1 in any orientation. Figure 6 also highlights the actin monomer adjacent to the monomer that directly binds S1 (white outline). Here, without Tn in the proposed location, it is feasible that S1 loop 3 can extend and potentially interact with actin helix 91−100, more specifically between the positively charged Lys572/574 of loop 3 and negatively charged Glu99/100 of actin (Figure 7), as previously stated by Rayment et al. (*24*). These amino acids appear to be significant for myosin function since they are highly conserved in vertebrate skeletal myosins (*24, 60*). This electrostatic interaction, however, may be obstructed by C-TnT,

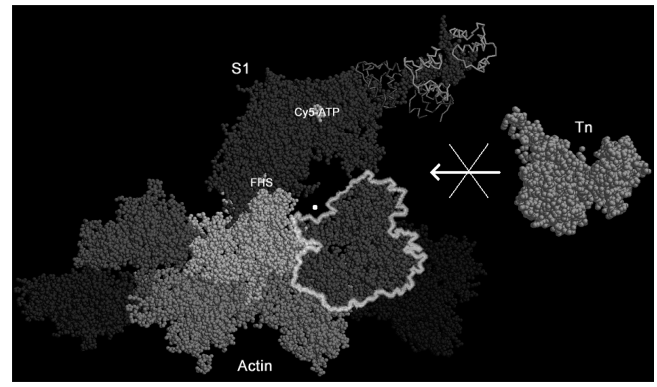

FIGURE 6: Location of C-TnT in an actomyosin atomic model. Previously, S1 was docked objectively with actin by Rayment et al. (*24*). This atomic model, designated as model 1, shows the location of C-TnT (white sphere) with respect to myosin S1 in the postpowerstroke state bound to the actin filament. It is clear that if Tn is placed at the specified location, this S1 configuration would be inhibited. Cy5-ATP and FHS are shown as space-filled structures indicating their relationship with the actomyosin complex. The N- and C-terminal of the actin monomer that directly binds S1 is at the interface of the two proteins, while the adjacent monomer (highlighted outline) also contains residues thought to be involved in S1 strong binding.

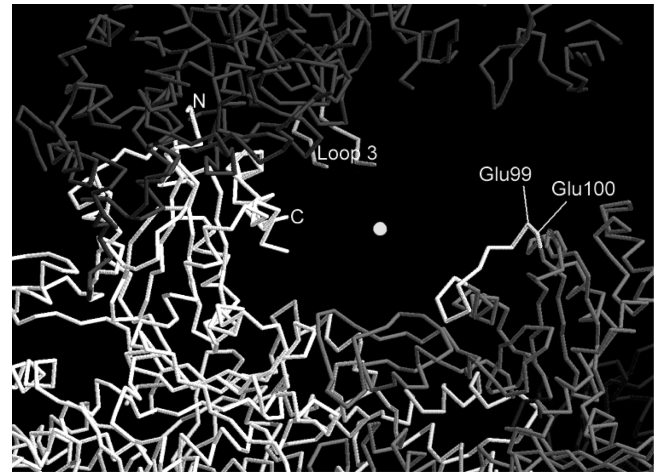

FIGURE 7: Potential TnT contact with myosin S1 and actin. A closer view of model 1 in Figure 6 shows possible interactions between myosin loop 3, C-TnT (white sphere), and actin helix Tyr91−Glu100, particularly of the actin monomer adjacent to the one that binds S1 (highlighted outline, Figure 6). More specifically, TnT may perturb the previously described interaction between loop 3 Lys572/574 and Glu99−Glu100. Note residues 572−574 are not mapped in the crystal structure due to their highly flexible nature. The N- and C-terminals of actin are visible at the S1−actin binding interface.

Table 2: Distance between C-TnT and Various Sites in Three Actomyosin Atomic Models

	atom[a]	site	LRET	model 1	model 2[a]	model 3
S1 Label						
Cy5-ATP	C^{α}	ATP binding (Trp131)	4.84	4.84	4.84	4.84
TMR	S (C^{α})	SH1 (Cys707)	4.49	4.49	4.49 (4.41)	4.49
FHS	N (C^{α})	actin binding (Lys553)	3.40	3.40	3.40 (2.90)	3.40
Protein/Motif						
actin monomer that binds S1	C^{α}	actin N-terminal (Glu2)		3.70 [4.32]	4.35 [1.55]	2.63 [4.42]
	C^{α}	actin C-terminal (Arg372)		1.56 [4.12]	4.30 [3.45]	1.38 [4.68]
actin helix	C^{α}	Ser350		2.30 [4.89]	3.27 [2.65]	1.58 [5.14]
	C^{α}	Thr351		1.92 [4.97]	3.17 [2.88]	1.21 [5.26]
	C^{α}	Phe352		1.95 [4.62]	3.51 [2.67]	1.24 [4.93]
	C^{α}	Gln353		1.87 [4.52]	3.62 [2.49]	1.18 [4.83]
	C^{α}	Gln354		1.50 [4.68]	3.50 [2.80]	0.81 [5.04]
	C^{α}	Met355		1.64 [4.42]	3.73 [2.80]	1.02 [4.80]
	C^{α}	Trp356		1.91 [4.16]	4.05 [2.45]	1.28 [4.51]
	C^{α}	Ile357		1.74 [4.15]	4.31 [2.53]	1.21 [4.54]
actin monomer adjacent to the right of the S1-binding monomer	C^{α}	Arg39		1.50	3.45	1.51
	C^{α}	His40		1.51	3.48	1.32
	C^{α}	Arg95		3.22	0.78	3.20
	C^{α}	Val96		3.24	0.71	3.29
	C^{α}	Ala97		3.05	0.80	3.14
S1 (loop 3)	C^{α}	Pro570		1.02	0.87	1.02
	C^{α}	Ala571		0.91	0.74	0.91
	C^{α}	Ala575		1.27	1.52	1.27

[a] Model 2 (*45*), PDB file 1ALM, contains only C^{α} coordinates; thus actual measurements to the Cys707 sulfur atom (S) and Lys553 terminal nitrogen atom (N), in parentheses, were calculated from model 1 using RasMol software. Square brackets indicate distance measurements to the actin monomer adjacent to the right of the S1-binding monomer (highlighted in Figure 6). Underlined values indicate the shortest distance to C-TnT within the specified motif.

thus implying that S1, actin, and Tn have to undergo structural changes to allow the formation of the rigor complex. Such structural changes have been implied before by Schröder et al. (*19*), where atomic models of S1 docked onto F-actin interpenetrated the contact region, suggesting that S1 must exhibit conformational changes to form the rigor complex.

Table 2 summarizes the distances (nm) observed between C-TnT and various sites in the three actomyosin atomic models. The close association of S1 loop 3 with C-TnT (0.7−1.5 nm) suggests direct contact between bound myosin heads and the Tn complex. Though loop 3 is comprised of residues 570−575, residues 572−574 are not accurately modeled by X-ray crystallography due to the highly flexible nature that is typical of loop regions. Consequently, it is conceivable that these missing residues may reside closer to C-TnT than the reported values in Table 2, yet the exact location would be expected to fluctuate given the highly mobile nature of the loop. A distance of about 1.5 nm is also observed with respect to either the N- or C-terminal of the actin monomer that binds directly to S1 or the adjacent actin monomer (highlighted in Figure 6). Model 2 shows C-TnT in closest proximity to actin Val96 (0.7 nm), which has previously been shown to interact with the hypertrophic cardiomyopathy (HCM) loop of myosin (*14*). Models 1 and 3 favor interaction between C-TnT and Gln354 of the actin helix that binds S1 (separated by 1.5 and 0.8 nm, respectively). This is consistent with other reports stating actin helix 350−358 participates in strong binding of S1 to actin. The close proximity of C-TnT to these regions suggests then that Tn may perturb these interactions and so alter the binding contacts of S1 to actin.

Possible Inhibitory Effects of Tn on Actomyosin Interactions. It has been shown before that each myosin head interacts with two actin monomers forming primary and secondary binding sites (*14, 18, 24*). Binding of myosin to actin is believed to first involve the formation of a weak ionic interaction and then a stronger stereospecific interaction. The weak ionic interaction is thought to be responsible for the ionic strength-dependent "weak binding" of myosin to actin, which is thought to be mediated between myosin Tyr626−Glu647 and actin Asp1−Glu4 and Asp24−Asp25 (*61*). The "strong binding" of myosin to actin is thought to occur via stereospecific contacts between myosin Pro529−Lys553 and actin Iso341−Gln354 and Ala144−Thr148. The presence of C-TnT near these regions indicated in Figure 6 and Table 2 suggests Tn may inhibit these contacts from being realized, particularly of those myosins binding adjacent to Tn. Therefore, it appears that the fraction of myosin molecules binding adjacent to Tn are likely to adopt different contacts with actin than those myosin molecules binding away from the Tn complex. Such behavior is consistent with the actomyosin atomic models showing the apparent inhibition of the S1 postpowerstroke state due to the steric hindrance imposed by the Tn complex. This is in accordance with other FRET measurements that support the S1 rigor state to bind near Tn, but not when the postpowerstroke state is induced (*62*). Also, Glu93, located near the junction of actin subdomains 1 and 2, and Cys374 at the C-terminal end of actin are thought to be involved in myosin binding (*63, 64*). These findings coincide well with the atomic models that show these residues at the actomyosin binding interface; however, the mapped location of Tn shows the complex could conceivably block the interactions and prevent myosin from assuming the postpowerstroke state and thus not participate in productive force generation. This is supported by the relatively short distances observed between C-TnT and actin C-terminal/helix 95−97 of the adjacent actin monomer (Table 2). Evidence supports that S1 possessing the longer ELC isoform (A1) binds actin with higher affinity

than S1 with the shorter isoform (A2) and may function to stabilize actin−actin contacts to promote actin polymerization *in vitro* (*22*). ELCA1 has been shown to bind actin 360−363 (*65, 66*), which is close to the aforementioned actin helix 350−358, thought to contribute to S1 strong binding. In our experiments then, the fraction of S1 possessing ELCA1 may not be able to interact with actin as efficiently due to the perturbation from C-TnT, thus preventing the enhanced binding of S1-ELCA1 from being realized. How this may affect the swinging motion of the lever arm and the implications of the two different ELC isoforms remain to be discovered.

Movement of C-TnT. Several studies have attempted to reveal the position and orientation of Tn on the actin filament using electron microscopy. For example, Lehman et al. (*11*) support the interaction of the globular head (N-terminal) domain of Tn with Tm and the extreme periphery of subdomains 1 and 2 of the actin monomer in the absence of calcium. The association with actin, however, is abolished upon the addition of calcium. In the present study, data support that the C-terminal region of Tn does not shift appreciably upon the addition of calcium. This finding correlates with Lehman's data since they refer to a so-called stalk region of Tn, which is believed to include the C-terminal region of TnT that does not shift significantly when calcium is added. Unlike most studies, our LRET measurements consider the effect of S1 binding to actin, which may restrict the motion of C-TnT even when myosin binds weakly (no calcium) and strongly (with calcium) to actin. Besides effects on TnT, other studies support that, in the absence of calcium, TnI forms a C-clamp configuration around the N- and C-terminal region of actin and, together with Tm, inhibits muscle contraction (*60, 67, 68*). It is feasible, though, that Tn alone, i.e., without Tm, can sterically hinder binding of S1 near the N-terminal region of actin, which would not allow myosin to proceed to the postpowerstroke state and generate force (implied in Figure 6).

Possible Physiological Role of Tn Inhibiting the Powerstroke. Collectively, the results suggest the Tn complex inhibits myosin molecules that bind adjacent to it from obtaining the postpowerstroke state and, thus, would not produce force. This is contrary to myosins that bind further away from the Tn complex on the actin filament, which would consequently be expected to produce force. Based on a proposed hypothesis by Xu and Root (*54*) that states only one of a variety of S1 neck-region orientations preferentially binds actin to allow the transition to the strong binding state, our data suggest that either (1) this selected conformation is not assumed when binding near Tn, thus the postpowerstroke state is not realized, or (2) this selected conformation can bind adjacent to Tn but is physically inhibited from achieving the postpowerstroke state due to steric hindrance posed by Tn. Though it is not clear, it is possible that this apparent differential behavior of myosin binding to actin, i.e., those myosins binding adjacent to Tn versus those binding elsewhere, contributes to a regulatory mechanism that was not obvious before. It is conceivable that myosin binding adjacent to Tn may function as a mechanical sensor and drag along the actin filament to dampen the effect of sliding filaments. Also, potential interactions with Tn and Tm suggest it could also play a regulatory role in sensing and controlling the extent of contraction, while maintaining the sarcomere length within optimal limits in concert with other structural proteins, such as titin.

While the data presented here imply Tn does not allow the formation of the postpowerstroke state, it is not yet possible to demonstrate whether it occurs in muscle fibers. Further studies are required to (a) functionally determine whether the myosin postpowerstroke state is inhibited due to the physical presence of the Tn complex and (b) provide more evidence that productive binding occurs in regions away from the Tn complex, where the postpowerstroke state is not apparently inhibited.

In summary, the interaction of myosin heads with the thin filament involves differential binding of S1 where some myosin heads can bind very close to the Tn complex, while others bind relatively farther away. In the latter condition, myosin can easily attain the powerstroke state via swinging of the lever arm, while the powerstroke of myosin binding adjacent to Tn appears to be inhibited due to the physical presence of the complex. This is supported by mapping the C-TnT region in current atomic models of actomyosin that do not appear to readily accommodate the LRET-derived position of Tn. The determined location of the Tn complex near loop 3 of myosin suggests a potential zone for direct contact with the myosin. Although the position of C-TnT was determined using reconstituted thin filaments, measurements in myofibrils confirm that this close proximity also occurs when the full array of contractile proteins are present.

ACKNOWLEDGMENT

We thank Dr. Zhiling Zhang for preparing the chicken breast TnT used in this study.

REFERENCES

1. Gordon, A. M., Homsher, E., and Regnier, M. (2000) Regulation of contraction in striated muscle. *Physiol. Rev. 80*, 853–924.
2. Holmes, K. C., Popp, D., Gebhard, W., and Kabsch, W. (1990) Atomic model of the actin filament. *Nature 347*, 44–49.
3. McKillop, D. F., and Geeves, M. A. (1993) Regulation of the interaction between actin and myosin subfragment 1: evidence for three states of the thin filament. *Biophys. J. 65*, 693–701.
4. Ebashi, S., Endo, M., and Ohtsuki, I. (1969) Control of muscle contraction. *Q. Rev. Biophys. 2*, 351–384.
5. Greaser, M. L., and Gergely, J. (1971) Reconstitution of troponin activity from three protein components. *J. Biol. Chem. 246*, 4226–4233.
6. Pearlstone, J. R., Sykes, B. D., and Smillie, L. B. (1997) Interactions of structural C and regulatory N domains of troponin C with repeated sequence motifs in troponin I. *Biochemistry 36*, 7601–7606.
7. Perry, S. V. (1998) Troponin T: genetics, properties and function. *J. Muscle Res. Cell Motil. 19*, 575–602.
8. Stefancsik, R., Jha, P. K., and Sarkar, S. (1998) Identification and mutagenesis of a highly conserved domain in troponin T responsible for troponin I binding: potential role for coiled coil interaction. *Proc. Natl. Acad. Sci. U.S.A. 95*, 957–962.
9. Van Eyk, J. E., Thomas, L. T., Tripet, B., Wiesner, R. J., Pearlstone, J. R., Farah, C. S., Reinach, F. C., and Hodges, R. S. (1997) Distinct regions of troponin I regulate Ca^{2+}-dependent activation and Ca^{2+} sensitivity of the acto-S1-TM ATPase activity of the thin filament. *J. Biol. Chem. 272*, 10529–10537.
10. Gorga, J. A., Fishbaugher, D. E., and VanBuren, P. (2003) Activation of the calcium-regulated thin filament by myosin strong binding. *Biophys. J. 85*, 2484–2491.
11. Lehman, W., Rosol, M., Tobacman, L. S., and Craig, R. (2001) Troponin organization on relaxed and activated thin filaments revealed by electron microscopy and three-dimensional reconstruction. *J. Mol. Biol. 307*, 739–744.
12. Bacchiocchi, C., Graceffa, P., and Lehrer, S. S. (2004) Myosin-induced movement of alphaalpha, alphabeta, and betabeta smooth

muscle tropomyosin on actin observed by multisite FRET. *Biophys. J. 86*, 2295–2307.
13. Swartz, D. R., and Moss, R. L. (1992) Influence of a strong-binding myosin analogue on calcium-sensitive mechanical properties of skinned skeletal muscle fibers. *J. Biol. Chem. 267*, 20497–20506.
14. Holmes, K. C., Schröder, R. R., Sweeney, H. L., and Houdusse, A. (2004) The structure of the rigor complex and its implications for the powerstroke. *Philos. Trans. R. Soc. London, Ser. B: Biol. Sci. 359*, 1819–1828.
15. Root, D. D., Stewart, S., and Xu, J. (2002) Dynamic docking of myosin and actin observed with resonance energy transfer. *Biochemistry 41*, 1786–1794.
16. Root, D. D. 2002a The dance of actin and myosin: a structural and spectroscopic perspective. *Cell Biochem. Biophys. 37*, 111–139.
17. Labbé, J. P., Boyer, M., Mejean, C., Roustan, C., and Benyamin, Y. (1993) Localization of two myosin-subfragment-1 binding contacts in the 96−132 region of actin subdomain-1. *Eur. J. Biochem. 215*, 17–24.
18. Labbé, J. P., Boyer, M., and Benyamin, Y. (1995) Two identical hydrophobic clusters are present on the same actin monomer: interaction between one myosin subfragment-1 and two actin monomers. *FEBS Lett. 373*, 221–224.
19. Schröder, R. R., Manstein, D. J., Jahn, W., Holden, H., Rayment, I., Holmes, K. C., and Spudich, J. A. (1993) Three-dimensional atomic model of F-actin decorated with *Dictyostelium* myosin S1. *Nature 364*, 171–174.
20. Milligan, R. A., and Flicker, P. F. (1987) Structural relationships of actin, myosin, and tropomyosin revealed by cryo-electron microscopy. *J. Cell Biol. 105*, 29–39.
21. Flicker, P. F., Phillips, G. N., and Cohen, C. (1982) Troponin and its interactions with tropomyosin. An electron microscope study. *J. Mol. Biol. 234*, 495–501.
22. Milligan, R. A., Whittaker, M., and Safer, D. (1990) Molecular structure of F-actin and location of surface binding sites. *Nature 348*, 217–221.
23. Lorenz, M., Popp, D., and Holmes, K. C. (1993) Refinement of the F-actin model against X-ray fiber diffraction data by the use of a directed mutation algorithm. *J. Mol. Biol. 234*, 826–836.
24. Rayment, I., Holden, H. M., Whittaker, M., Yohn, C. B., Lorenz, M., Holmes, K. C., and Milligan, R. A. 1993a Structure of the actin-myosin complex and its implications for muscle contraction. *Science 261*, 58–65.
25. Kimura, C., Maeda, K., Maeda, Y., and Miki, M. (2002) Ca(2+)- and S1-induced movement of troponin T on reconstituted skeletal muscle thin filaments observed by fluorescence resonance energy transfer spectroscopy. *J. Biochem. 132*, 93–102.
26. Miki, M., Kobayashi, T., Kimura, H., Hagiwara, A., Hai, A., and Maéda, Y. 1998a Ca^{2+}-induced distance change between points on actin and troponin in skeletal muscle thin filaments estimated by fluorescence resonance energy spectroscopy. *J Biochem. 123*, 324–331.
27. Miki, M., Miura, T., Sano, K., Kimura, H., Kondo, H., Ishida, H., and Maéda, Y. 1998b Fluorescence resonance energy transfer between points on tropomyosin and actin in skeletal muscle thin filaments: does tropomyosin move. *J. Biochem. 123*, 1104–1111.
28. Miki, M., Hai, H., Saeki, K., Shitaka, Y., Sano, K., Maéda, Y., and Wakabayashi, T. (2004) Fluorescence resonance energy transfer between points on actin and the C-terminal region of tropomyosin in skeletal muscle thin filaments. *J. Biochem. 136*, 39–47.
29. Vinogradova, M. V., Stone, D. B., Malanina, C. G., Karatzaferi, C., Cooke, R., Mendelson, R. A., and Fletterick, R. J. (2005) Ca(2+)-regulated structural changes in troponin. *Proc. Natl. Acad. Sci. U.S.A. 102*, 5038–5043.
30. Takeda, S., Yamashita, A., Maeda, K., and Maéda, Y. (2003) Structure of the core domain of human cardiac troponin in the Ca(2+)-saturated form. *Nature 424*, 35–41.
31. Jin, J.-P., and Root, D. D. (2000) Modulation of troponin T molecular conformation and flexibility by metal ion binding to the N-terminal variable region. *Biochemistry 39*, 11702–11713.
32. Godfrey, J. E., and Harrington, W. F. (1970) Self-association in the myosin system and high ionic strength. I. Sensitivity of the interaction to pH and ionic environment. *Biochemistry 9*, 886–895.
33. Weeds, A. G., and Pope, B. (1977) Studies on the chymotryptic digestion of myosin: effects of divalent cations on proteolytic susceptible. *J. Mol. Biol. 111*, 129–157.
34. Spudich, J. A., and Watt, S. (1971) The regulation of rabbit skeletal muscle contraction. I. Biochemical studies of the interaction of the tropomyosin-troponin complex with actin and the proteolytic fragments of myosin. *J. Biol. Chem. 246*, 4866–4871.
35. Zhang, Z., Jin, J.-P., and Root, D. D. (2004) Binding of calcium ions to an avian flight muscle troponin T. *Biochemistry 43*, 2645–2655.
36. Smillie, L. B. (1982) Preparation and identification of α- and β-tropomyosins. *Methods Enzymol. 85*, 234–241.
37. Potter, J. D. (1982) Preparation of troponin and its subunits. *Methods Enzymol. 85*, 244–260.
38. Xu, J., and Root, D. D. (1998) Domain motion between the regulatory light chain and the nucleotide site in skeletal myosin. *J. Struct. Biol. 123*, 150–161.
39. Root, D. D., Cheung, P., and Reisler, E. (1991) Catalytic cooperativity induced by SH1 labeling of myosin filaments. *Biochemistry 30*, 286–294.
40. Bertrand, R., Derancourt, J., and Kassab, R. (1995) Production and properties of skeletal myosin subfragment 1 selectively labeled with fluorescein at lysine-553 proximal to the strong actin-binding site. *Biochemistry 34*, 9500–9507.
41. Root, D. D. (1997) In situ molecular association of dystrophin with actin revealed by sensitized emission immuno-resonance energy transfer. *Proc. Natl. Acad. Sci. U.S.A. 94*, 5685–5690.
42. Shiraishi, F., Kambara, M., and Ohtsuki, I. (1992) Replacement of troponin components in myofibrils. *J. Biochem. 111*, 61–65.
43. Holmes, K. C., Tirion, M., Popp, D., Lorenz, M., Kabsch, W., and Milligan, R. A. (1993) A comparison of the atomic model of F-actin with cryo-electron micrographs of actin and decorated actin. *Adv. Exp. Med. Biol. 332*, 15–22.
44. Rayment, I., Rypniewski, W. R., Schmidt-Bäse, K., Smith, R., Tomchick, D. R., Benning, M. M., Winkelmann, D. A., Wesenberg, G., and Holden, H. M. 1993b Three-dimensional structure of myosin subfragment-1: a molecular motor. *Science 261*, 50–58.
45. Mendelson, R., and Morris, E. P. (1997) The structure of the acto-myosin subfragment 1 complex: results of searches using data from electron microscopy and X-ray crystallography. *Proc. Natl. Acad. Sci. U.S.A. 94*, 8533–8538.
46. Root, D. D. 2002b A computational comparison of the atomic models of the actomyosin interface. *Cell Biochem. Biophys. 37*, 97–110.
47. Getz, E. B., Cooke, R., and Selvin, P. R. (1998) Luminescence resonance energy transfer measurements in myosin. *Biophys. J. 74*, 2451–2458.
48. Wolff-Long, V. L., Tao, T., and Lowey, S. (1995) Proximity relationships between engineered cysteine residues in chicken skeletal myosin regulatory light chain. *J. Biol. Chem. 270*, 31111–31118.
49. Funatsu, T., Harada, Y., Tokunaga, M., Saito, K., and Yanagida, T. (1995) Imaging of single fluorescent molecules and individual ATP turnovers by single myosin molecules in aqueous solution. *Nature 374*, 555–559.
50. Liou, Y.-M., and Chao, H.-L. (2007) Fluorescence spectroscopic analysis of the proximity changes between the central helix of troponin C and the C-terminus of troponin T from chicken skeletal muscle. *Biochim. Biophys. Acta 1774*, 466–473.
51. Root, D. D., and Reisler, E. (1992) Cooperativity of thiol-modified myosin filaments: ATPase and motility assays of myosin function. *Biophys. J. 63*, 730–740.
52. Maruta, S., Henry, G. D., Sykes, B. D., and Ikebe, M. (1993) Formation of the stable myosin-ADP-aluminum fluoride and myosin-ADP-beryllium fluoride complexes and their analysis using ^{19}F NMR. *J. Biol. Chem. 268*, 7093–7100.
53. Werber, M. M., Peyser, M. Y., and Muhlrad, A. (1992) Characterization of stable beryllium fluoride, aluminum fluoride, and vanadate containing myosin subfragment 1-nulcleotide complexes. *Biochemistry 31*, 7190–7197.
54. Xu, J., and Root, D. D. (2000) Conformational selection during weak binding at the actin and myosin interface. *Biophys. J. 79*, 1498–1510.
55. Moss, D. J., and Trentham, D. R. (1983) Distance measurement between the active site and cysteine-177 of the alkali one light chain of subfragment 1 from rabbit skeletal muscle. *Biochemistry 22*, 5261–5270.
56. Greene, L. E., and Eisenberg, E. (1980) Cooperative binding of myosin subfragment-1 to the actin-troponin-tropomyosin complex. *Proc. Natl. Acad. Sci. U.S.A. 77*, 2616–2620.
57. Borejdo, J., Shepard, A., Dumka, D., Akopova, I., Talent, J., Malka, A., and Burghardt, T. P. (2004) Changes in orientation of actin during contraction of muscle. *Biophys. J. 86*, 2308–2317.

58. Chalovich, J. M., and Eisenberg, E. (1982) Inhibition of actomyosin ATPase activity by troponin-tropomyosin without blocking the binding of myosin to actin. *J. Biol. Chem. 257*, 2432–2437.
59. Maytum, R., Lehrer, S. S., and Geeves, M. A. (1999) Cooperativity and switching within the three-state model of muscle regulation. *Biochemistry 38*, 1102–1110.
60. Johara, M., Toyoshima, Y. Y., Ishijima, A., Kojima, H., Yanagida, T., and Sutoh, K. (1993) Charge-reversion mutagenesis of *Dictyostelium* actin to map the surface recognized by myosin during ATP-driven sliding motion. *Proc. Natl. Acad. Sci. U.S.A. 90*, 2127–2131.
61. Brenner, B., Schoenberg, M., Chalovich, J. M., Greene, L. E., and Eisenberg, E. (1982) Evidence for cross-bridge attachment in relaxed muscle at low ionic strength. *Proc. Natl. Acad. Sci. U.S.A. 79*, 7288–7291.
62. Coffee, P. G., and Root, D. D. (2007)Hindrance of the myosin power stroke posed by the proximity to the troponin complex identified using a novel LRET fluorescent nanocircuit, Master's Thesis.
63. Razzaq, A., Schmitz, S., Veigel, C., Molloy, J. E., Geeves, M. A., and Sparrow, J. C. (1999) Actin residue Glu93 is identified as an amino acid affecting myosin binding. *J. Biol. Chem. 274*, 28321–28328.
64. Moens, P. D. J., and dos Remedios, C. G. (1997) A conformational change in F-actin when myosin binds: fluorescence resonance energy transfer detects an increase in the radial coordinate of Cys374. *Biochemistry 36*, 7353–7360.
65. Sutoh, K. (1982) Identification of myosin-binding sites on the actin sequence. *Biochemistry 21*, 3654–3661.
66. Trayer, I. P., Trayer, H. R., and Levine, B. A. (1987) Evidence that the N-terminal region of A1-light chain of myosin interacts directly with the C-terminal region of actin. A proton magnetic resonance study. *Eur. J. Biochem. 164*, 259–266.
67. Narita, A., Yasanuga, T., Ishikawa, T., Mayanagi, K., and Wakabayashi, T. (2001) Ca(2+)-induced switching of troponin and tropomyosin on actin filaments as revealed by electron cryomicroscopy. *J. Mol. Biol. 308*, 241–261.
68. Murakami, K., Yumoto, F., Ohki, S. Y., Yasunaga, T., Tanokura, M., and Wakabayashi, T. (2005) Structural basis for Ca^{2+}-regulated muscle relaxation at interaction sites of troponin with actin and tropomyosin. *J. Mol. Biol. 352*, 178–201.

BI801554M